Electron Paramagnetic Resonance Study of the Pyrochlore Iridate $Gd_2Ir_2O_7$

Hui Han,[1,2] Lei Zhang,[1,*] Hui Liu,[1] Langsheng Ling,[1] Wei Tong,[1] Youming Zou,[1] Min Ge,[3] Jiyu Fan,[4] Changjin Zhang,[1] Li Pi,[1,3] and Yuheng Zhang[1,3]

[1]*High Magnetic Field Laboratory, Chinese Academy of Sciences, Hefei 230031, China*

[2]*School of Physics and Material Science,*
Anhui University, Hefei 230601, China

[3]*Hefei National Laboratory for Physical Sciences at the Microscale,*
University of Science and Technology of China, Hefei 230026, China

[4]*Department of Applied Physics, Nanjing University of*
Aeronautics and Astronautics, Nanjing 210016, China

(Dated: April 8, 2015)

Abstract

The pyrochlore iridate $Gd_2Ir_2O_7$ has been investigated by means of the electron paramagnetic resonance (EPR) spectroscopy. A magnetic transition at $T^* \sim 20$ K is found in addition to the transition at $T_C \sim 130$ K, which has not been reported previously. The phase transition at T_C, which corresponds to a resistivity transition, is resulted from the long-range spin ordering of Ir^{4+} ions in all-in/all out state. However, the magnetic transition at T^*, which is regardless of resistivity transition, is not caused by Ir^{4+} but Gd^{3+} ions. Both of the magnetic transitions are irrelevant to the lattice distortion. We suggest that the competition between the enhanced paramagnetism of Gd^{3+} ions and the $f - d$ interaction should be responsible for the magnetic transition at T^*.

---
*Corresponding author. Email: zhanglei@hmfl.ac.cn (L. Zhang)

1

I. INTRODUCTION

The iridium-based compounds with $5d$ outer-shell electrons provide a prototype to investigate the interplay between the spin-orbit coupling, electronic correlations, and band topology due to the comparability of spin-orbit coupling energy ($U_{so} \sim 0.3 - 1$ eV), electronic correlation energy ($U_{ee} \sim 0.4 - 2$ eV), and crystal field splitting energy ($U_{CF} \sim 1 - 5$ eV) [1, 2, 3, 4, 5]. The competition and collaboration between these energies result in multiple ground states, such as quantum criticality state, charge-orbital density wave, orbitally-driven Peierls phase, and superconductivity [6, 7, 8, 9, 10]. Recently, the iridate pyrochlore oxides $A_2Ir_2O_7$ (A = lanthanides or Y, Yb and Bi *etc*) are paid great attention due to the theoretical predictions of exotic phases including axion insulator, strong topological insulator, and Weyl semimetal [11, 12, 13, 14, 15, 16, 17]. Pyrochlore $A_2Ir_2O_7$ is composed of a network of corner-shared tetrahedra, whose vertices are occupied by spins [18, 19]. The spins on vertices of the tetrahedron form geometrical frustration, which enhance the spin fluctuation. Consequently, the degeneracy of ground states is further increased. The $A_2Ir_2O_7$, except $Pr_2Ir_2O_7$ [20], commonly exhibits a second-order insulating phase transition with a magnetic transition into a long-range all-in/all-out antiferromagnetic state formed by spins of Ir^{4+} ions, as shown in the inset of Fig. 1 [21, 22, 23, 24]. Some of the rare-earth ions on A-sites form spin ordering at low temperatures, such as $Nd_2Ir_2O_7$ and $Eu_2Ir_2O_7$ [25, 26, 27]. When A^{3+} ions are magnetic, the magnetic moments from A-sites would modulate the magnetic ordering on B-sites. Moreover, the possible $f - d$ exchange interaction between the Ir^{4+} and A^{3+} leads to even more complex magnetic structures [28]. Therefore, the investigation of $A_2Ir_2O_7$ with magnetic ions on A-sites is important to clarify the fundamental magnetic properties of this system.

As we know, the magnetic moments of Gd^{3+} ions are strong in the compounds, where the Gd^{3+} ions on A-sites would introduce strong modulation on the magnetic ordering on B-sites in $A_2Ir_2O_7$ system. In this work, the magnetic behavior of $Gd_2Ir_2O_7$ has been investigated by the electron paramagnetic resonance (EPR) spectroscopy. A magnetic transition at $T^* \sim 20$ K is found in addition to the magnetic transition at $T_C \sim 130$ K, which has not been reported previously. We suggest that the competition between the Gd^{3+} ions and the $f - d$ interaction should be responsible for the magnetic transition at T^*.

2

II. EXPERIMENT

A polycrystalline sample of $Gd_2Ir_2O_7$ was synthesized by the solid-state reaction method. The starting materials, powders of Gd_2O_3 (purity 99.9%) and IrO_2 (99.99%) were mixed thoroughly according to the stoichiometric ratio of 1 : 2.1. The mixed powder was sintered at 1373 K for 4 days with several intermediate grindings. After adding 10 % IrO_2, the powder sample was pressed into pellet. Then, the sample was sintered at 1423 K for another 4 days.

The structure and phase purity were checked by the Rigaku-TTR3 X-ray diffractometer with high-intensity graphite monochromatized Cu Kα radiation. The resistivity measurement was carried out by conventional four-probe method using a Physical Property Measurement System (Quantum Design PPMS). The Raman scattering measurements were performed using a Horiba Jobin Yvon T64000 Micro-Raman instrument with a Kr$^+$-Ar$^+$ mixed gas laser ($\lambda = 514.5$ nm) as an excitation source in a backscattering geometry. The EPR measurement was carried out at selected temperatures using a Bruker EMX-plus model spectrometer operating at X-band frequency ($\nu \approx 9.4$ GHz). The magnetization was measured by a Magnetic Property Measurement System (Quantum Design MPMS 7T-XL) with a superconductive quantum interference device (SQUID). The isothermal magnetization $[M(H)]$ curves were measured after the sample heated well above T_C.

III. RESULTS AND DISCUSSION

Figure 1 shows the powder X-ray diffraction (XRD) pattern for $Gd_2Ir_2O_7$ at 300 K, which is refined by the Rietveld method. The refined XRD result indicates that the sample is single phase with cubic cell belonging to space group $Fd\bar{3}m$, in agreement with the previous report [22]. Figure 2 (a) gives the temperature dependence of resistivity $[\rho(T)]$ for $Gd_2Ir_2O_7$, where the inset depicts that on the $\lg - \lg$ scale. An upturn is found from the inset of Fig. 2 (a) at $T_C \sim 124$ K, in agreement with the previous report [29]. As suggested by J. J. Ishikawa, *et al.*, the $\lg \rho$ vs $T^{-\alpha}$ exhibits a linear relation with $\alpha = 1/4$ at low temperature in $Eu_2Ir_2O_7$ [30]. Figure 2 (b) gives the $\lg \rho$ vs $T^{-1/4}$ for $Gd_2Ir_2O_7$, which exhibits a linear relation at low temperature. However, J. J. Ishikawa, *et al.*, suggest that these systems are not typical Mott insulators for the reason that the charge gap is much larger than the transition

3

temperature. The inset of Fig. 2 (b) depicts the derivative $\lg \rho(T)$ vs $T^{-1/4}$, which clearly demonstrates the different conductive mechanisms below and above T_C. It is noticed that $\rho(T)$ of $Y_2Ir_2O_7$ also obeys the $T^{-1/4}$ law below T_C [31], which indicates that the conductive mechanism of the $A_2Ir_2O_7$ system is determined by the Ir^{4+} ions on the B-sites rather than the ions on A-sites. Figure 2 (c) gives the Raman spectra at selected temperatures from 200 to 800 cm^{-1}, which are sensitive to detect the phonon coupling. Six peaks are found, which are corresponding to the active Raman modes: T_{2g}^1, P_1, P_2, A_{1g}, T_{2g}^2, and P_3 [32]. With temperature decreasing, no changes happen to these active Raman modes, indicating no change of phonon coupling.

The EPR spectroscopy, which is an effective means to detect the micro-magnetism, is performed to clarify the magnetic transitions in $Gd_2Ir_2O_7$. Figure 3 (a) shows derivative EPR spectra (dP/dH) (P is the integral EPR intensity) for $Gd_2Ir_2O_7$ at selected temperatures. With the decrease of temperature, changes occur to the EPR spectra gradually. It is noticed that there exist two kinds of paramagnetic ions in $Gd_2Ir_2O_7$ (Gd^{3+} ions on the A-sites and Ir^{4+} on the B-sites), both of which can produce EPR signals. Therefore, the most important problem is to determine which paramagnetic ions produce the EPR signals. Figure 3 (b) gives the EPR spectra for $Y_2Ir_2O_7$ and $Gd_2Ir_2O_7$ at 2 K for comparison. Because the Y^{3+} ions on A-sites are non-magnetic in the iso-structural $Y_2Ir_2O_7$, the EPR signals only originate from Ir^{4+} ions [31, 33]. The EPR spectrum of $Y_2Ir_2O_7$ is very weak compared with that of $Gd_2Ir_2O_7$, as seen in Fig. 3 (b). Therefore, it can be concluded that the strong EPR signals in $Gd_2Ir_2O_7$ are not from Ir^{4+} but from Gd^{3+} ions. In fact, the outer-shell electronic configuration of a Gd^{3+} ion is $4f^7$ providing an effective moment of 7.94 μ_B [34], which is much stronger than 1.73 μ_B of a Ir^{4+} ion.

Figure 4 (a), (b), and (c) show the temperature dependence of EPR parameters for $Gd_2Ir_2O_7$, including the resonance field H_r and corresponding g-factor, the height of the absorption peak, and the peak-to-peak linewidth ΔH_{pp}. As shown in Fig. 4 (a), H_r (defined as the H at $dP/dH = 0$) exhibits a dramatic increase below $T_C \sim 130$ K to the maximum value at $T^* \sim 20$ K. Then H_r decreases with temperature cooling below 20 K. The corresponding g-factor is calculated as $g = h\nu/\mu_B H_r$ (where h is the Planck constant, $\nu \approx 9.4$ GHz is the frequency of the used microwave, and μ_B is the Bohr magneton). It can be seen that g-factor approaches 2 above 130 K. As we know, the g-factor of a free paramagnetic spin is 2.003 [35]. Therefore, the g-factor above 130 K indicates a good paramagnetic be-

4

havior, which is in good agreement with the reported linear $M^{-1}(T)$ curve [23]. However, g-factor decreases below 130 K reaching the minimum value at 20 K. The decrease of the g-factor usually indicates spin coupling with the surrounding environment. With further decrease of temperature, g-factor increases to about 2 below 20 K. Correspondingly, the height of the EPR spectra exhibit a peak at 130 K, and rise below 20 K, as shown in Fig. 4 (b). As we know, the ΔH_{pp}, defined by the peak-to-peak linewidth, can directly reflect the coupling effect. It can be seen from Fig. 4 (c) that ΔH_{pp} increases with the decrease of temperature below 130 K and reaches the maximum at 20 K. The increase of ΔH_{pp} is usually caused by the broadening of linewidth of the EPR spectrum. The coupling of the paramagnetic ions with the surrounding would increases the relaxation time, which in turn increases the linewidth ΔH_{pp}. Therefore, the increase of ΔH_{pp} suggests the enhancement of coupling between the paramagnetic Gd^{3+} ions with surroundings. However, it is noticed that ΔH_{pp} decreases with the decrease of temperature below 20 K, which indicates the coupling is drastically weakened. All the EPR parameters approach paramagnetic characteristic at low temperature, indicating the enhancement of paramagnetism below T^*.

The isothermal magnetization $[M(H)]$ at selected temperatures are shown in Fig. 5. All the $M(H)$ curves exhibit paramagnetic behaviors, confirming the paramagnetic behavior indicated by the EPR spectra. The inset of Fig. 5 plots the magnified $M(H)$ at 2 K in lower field region, where no ferromagnetic hint is observed. The $M(H)$ curves indicate that the ferromagnetic ordering should be excluded in $Gd_2Ir_2O_7$, which is different from that in $Y_2Ir_2O_7$ [33]. The effective moment $\mu_{eff} = 11.8\ \mu_B/(f.u.)$ is obtained by the Curie paramagnetic law ($C = N\mu_{eff}^2/3k_B$, where N and k_B are the Avogadro and Boltzmann constants, μ_{eff} is the effective moment). It should be mentioned that the effective moment of Ir^{4+} is 1.73 $\mu_B/(Ir)$. Therefore, the main magnetic behavior is determined by Gd^{3+} ions, confirming the conclusion of the EPR results.

Figure 6 (a) shows the double integrated intensity I_{EPR} for $Gd_2Ir_2O_7$, which exhibits two peaks located at ~ 130 K and ~ 20 K, respectively. The reciprocal of I_{EPR} as a function of T is depicted in Fig. 6 (b), which shows that the $I_{EPR}^{-1}(T)$ above T_C is linearly dependent on the temperature consistent with the $M^{-1}(T)$ curve [23]. The temperature dependence of specific heat $[C/T]$ under $H = 50$ Oe is also shown in the inset of Fig. 6 (a), which exhibits an upturn below 20 K. The $C/T(T)$ curve for $Gd_2Ir_2O_7$ is similar to those of $Sm_2Ir_2O_7$ and $Nd_2Ir_2O_7$ [22, 23]. The anomaly in $Sm_2Ir_2O_7$ and $Nd_2Ir_2O_7$ is attributed to the tail of a Schottky

5

anomaly due to the crystalline electric field ground state doublet [23]. However, there is no upturn in the C/T for $Eu_2Ir_2O_7$ at low temperatures because Eu^{3+} has the ground state multiplet of $J = 0$ [23]. Therefore, the C/T curve of $Gd_2Ir_2O_7$ confirms that the anomaly below 20 K is attributed to Gd^{3+} ions. Apparently, there are two magnetic transitions for $Gd_2Ir_2O_7$ with the decrease of temperature. The transition at $T_C \sim 130$ K corresponds to the resistivity transition, while that at $T^* \sim 20$ K is only a magnetic transition. The transition at T_C is caused by Ir^{4+} ions on the B-sites, which occurs commonly in the $A_2Ir_2O_7$ systems. As we know, the spins of Ir^{4+} ions undergo an all-in/all-out transition, which is corresponding to the transport transition. The transition at T^* is caused by the Gd^{3+} ions on the A-sites, which is just a magnetic transition. Generally, the decrease of I_{EPR} indicates the reduction of the number of paramagnetic ions. The first decrease of I_{EPR} just below T_C is caused by the formation of the spin ordering of Ir^{4+} ions. The second decrease of I_{EPR} below T^* should be attributed to the reduced number of paramagnetic Gd^{3+} ions.

As indicated by the above experiment results, the spin ordering of Gd^{3+} ions should be excluded. Meanwhile, the $f-d$ interaction should be considered in the $Gd_2Ir_2O_7$, which plays an import role in the magnetic behavior [23, 28, 29, 36]. The $f-d$ coupling is not established above T_C due to the strong thermal fluctuation. When the all-in/all-out transition occurs to Ir^{4+} ions at T_C, the $f-d$ interaction is established between the f-electrons of Gd^{3+} and the d-electrons of Ir^{4+} ions. Below T_C, with the decrease of temperature, the $f-d$ interaction become more and more stronger, which is supported by the EPR results in Fig. 4 (a) and Fig. 4 (c). As shown by the EPR spectra, the $f-d$ interaction is enhanced gradually with the decrease of temperature below T_C, which indicating that fluctuation exist for the ordered Ir^{4+} ions. On the other hand, the paramagnetism of Gd^{3+} is also enhanced with the decrease of temperature according to the Curie law ($\chi = C/T$), which is confirmed by the EPR results in the Fig. 4 (a) and Fig. 4 (c). This enhancement of paramagnetism as $1/T$ is called Curie tail effect [37]. Thus, competition should exist between the enhanced paramagnetism and the $f-d$ interaction for the f-electrons. With the decrease of temperature, the enhanced paramagnetism conquers the $f-d$ interaction, which results in the transition at T^*. Therefore, the EPR parameters exhibit a paramagnetic characteristic below T^*, including $g \approx 2$ and the decrease of H_{pp}. However, due to the $f-d$ interaction, a part of the spins of Gd^{3+} lost their paramagnetic characteristic, which results the decrease of I_{EPR} below T^*, as shown in Fig. 6 (a). In another word, although the

paramagnetism is enhanced, the number of paramagnetic ions is reduced. Moreover, because the $f - d$ interaction is established based on the formation of long-range all-in/all-out of Ir^{4+}, the suppression of the transition at T_C causes the consequent disappearance of the transition at T^*.

IV. CONCLUSION

In summary, the pyrochlore $Gd_2Ir_2O_7$ is investigated by means of EPR spectroscopy. A magnetic transition at $T^* \sim 20$ K is found in addition to the transition at $T_C \sim 130$ K. The phase transition at T_C, which corresponds to a resistivity transition, is attributed to the long-range ordering of Ir^{4+} in all-in/all out state. However, the magnetic transition at T^* is regardless of resistivity transition. Both of the magnetic transitions are irrelevant to the lattice distortion. We suggest that the competition between the enhanced paramagnetism of Gd^{3+} ions and the $f - d$ interaction should be responsible for the magnetic transition at T^*.

V. ACKNOWLEDGEMENTS

---

[1] J. Chaloupka, G. Jackeli, G. Khaliullin, Phys. Rev. Lett. **105,** 027204 (2010).

[2] J. P. Clancy, N. Chen, C. Y. Kim, W. F. Chen, K. W. Plumb, B. C. Jeon, T. W. Noh, Y. J. Kim, Phys. Rev. B **86,** 195131 (2012).

[3] G. Cao, T. F. Qi, L. Li, J. Terzic, V. S. Cao, S. J. Yuan, M. Tovar, G. Murthy, R. K. Kaul, Phys. Rev. B **88,** 220414(R) (2013).

[4] G. Cao, T. F. Qi, L. Li, J. Terzic, S. J. Yuan, L. E. DeLong, G. Murthy, R. K. Kaul, Phys. Rev. Lett. **112,** 056402 (2014).

[5] L. Li, P. P. Kong, T. F. Qi, C. Q. Jin, S. J. Yuan, L. E. DeLong, P. Schlottmann, G. Cao, Phys. Rev. B **87,** 235127 (2013).

[6] C. H. Kim, H. S. Kim, H. Jeong, H. Jin, J. Yu, Phys. Rev. Lett. **108,** 106401 (2012).

[7] Y. Tokiwa, J. J. Ishikawa, S. Nakatsuji, P. Gegenwart, Nat. Mater. **13,** 356 (2014).

[8] J. J. Yang, Y. J. Choi, Y. S. Oh, A. Hogan, Y. Horibe, K. Kim, B. I. Min, S. W. Cheong, Phys. Rev. Lett. **108,** 116402 (2012).

[9] L. Zhang, X. D. Zhu, L. S. Ling, C. J. Zhang, L. Pi, Y. H. Zhang, Philos. Mag. **94,** 439 (2014).

[10] P. G. Radaelli, Y. Horibe, M. J. Gutmann, H. Ishibashi, C. H. Chen, R. M. Ibberson, Y. Koyama, Y. S. Hor, V. Kiryukhin, S. W. Cheong, Nature (Lond.) **416,** 155 (2002).

[11] J. S. Gardner, M. J. P. Gingras, J. E. Greedan, Rev. Mod. Phys. **82,** 53 (2010).

[12] D. Pesin and L. Balents, Nat. Phys. **6,** 376 (2010).

[13] Y. Yamaji and M. Imada, Phys. Rev. X **4,** 021035 (2014).

[14] X. G. Wan, A. M.Turner, A. Vishwanath, S. Y. Savrasov, Phys. Rev. B **83,** 205101 (2011).

[15] B. J. Yang and Y. B. Kim, Phys. Rev. B **82,** 085111 (2010).

[16] W. W. Krempa and Y. B. Kim, Phys. Rev. B **85,** 045124 (2012).

[17] L. Hozoi, H. Gretarsson, J. P. Clancy, B. G. Jeon, B. Lee, K. H. Kim, V. Yushankhai, P. Fulde, D. Casa, T. Gog, J. Kim, A. H. Said, M. H. Upton, Y. J Kim, J. Brink, Phys. Rev. B **89,** 115111 (2014).

[18] M. A. Subramanian, G. Aravamudan, G. V. S. Rao, Prog. Solid State Chem. **15,** 55 (1983).

[19] M. C. Shapiro, Scott C. Riggs, M. B. Stone, C. R. de la Cruz, S. Chi, A. A. Podlesnyak, I. R. Fisher, Phys. Rev. B **85,** 214434 (2012).

[20] Y. Machida, S. Nakatsuji, S. Onoda, T. Tayama, T. Sakakibara, Nature (London) **463**, 210 (2010).

[21] N. Taira, M. Wakeshima, Y. Hinatsu, J. Phys.: Condens. Matter **13,** 5527 (2001).

[22] K. Matsuhira, M. Wakeshima, R. Nakanishi, T. Yamada, A. Nakamura, W. Kawano, S. Takagi, Y.Hinatsu, J. Phys. Soc. Jpn. **76,** 043706 (2007).

[23] K. Matsuhira, M. Wakeshima, Y. Hinatsu, S. Takagi, J. Phys. Soc. Jpn. **80,** 094701 (2011).

[24] H. Sagayama, D. Uematsu, T. Arima, K. Sugimoto, J. J. Ishikawa, E. O. Farrell, S. Nakatsuji, Phys. Rev. B **87,** 100403(R) (2013).

[25] S. M. Disseler, C. Dhital, T. C. Hogan, A. Amato, S. R. Giblin, C. Cruz, A. Daoud-Aladine, S. Wilson, M. J. Graf, Phys. Rev. B **85,** 174441 (2012).

[26] H. J. Guo, K. Matsuhira, I. Kawasaki, M. Wakeshima, Y. Hinatsu, I. Watanabe, Z. A. Xu, Phys. Rev. B **88,** 060411(R) (2013).

[27] S. R. Zhao, J. M. Mackie, D. E. MacLaughlin, O. O. Bernal, J. J. Ishikawa, Y. Ohta, S. Nakatsuji, Phys. Rev. B **83,** 180402(R) (2011).

[28] G. Chen and M. Hermele, Phys. Rev. B **86,** 235129 (2012).

[29] K. Matsuhira, M. Tokunaga, M. Wakeshima, Y. Hinatsu, S. Takagi, J. Phys. Soc. Jpn **82,** 023706 (2013).

[30] J. J. Ishikawa, E. C. T. OFarrell, S. Nakatsuji, Phys. Rev. B **85,** 245109 (2012).

[31] H. Liu, W. Tong, L. S. Ling, S. L. Zhang, R. R. Zhang, L. Zhang, L. Pi, C. J. Zhang, Y. H. Zhang, Solid State Commun. **179,** 1 (2014).

[32] T. Hasegawa, N. Ogita, K. Matsuhira, S. Takagi, M. Wakeshima, Y. Hinatsu, M. Udagawa, J. Phys.: Conf. Ser. **200,** 012054 (2010).

[33] W. K. Zhu, M. Wang, Seradjeh, Fengyuan Yang, S. X. Zhang, Phys. Rev. B **90,** 054419 (2014).

[34] P. Bonville, J. A. Hodges, M. Ocio, J. P. Sanchez, P. Vulliet, S. Sosin, D. Braithwaite: J. Phys.: Condens. Matter **15,** 7777 (2003).

[35] L. Zhang, W. Tong, J. Y. Fan, C. J. Zhang, L. Pi, S. Tan, Y. H. Zhang, Physica B **411,** 136 (2013).

[36] S. M. Disseler, S. R. Giblin, C. Dhital, K. C. Lukas, S. D. Wilson, M. J. Graf, Phys. Rev. B **87,** 060403(R) (2013).

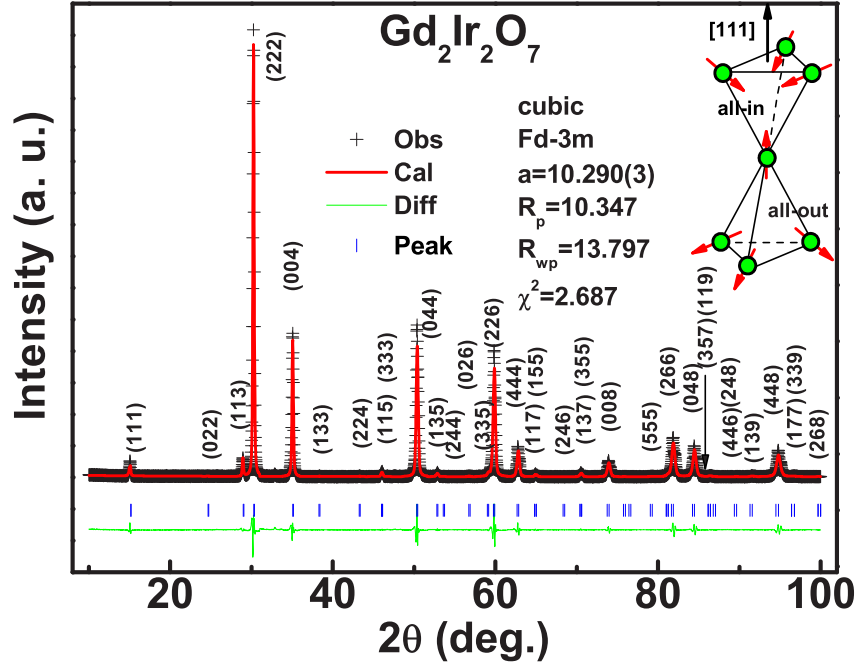[37] L. Zhang, H. C. Lei, X. D. Zhu, W. Tong, C. J. Zhang, Y. H. Zhang, C. Petrovic, Philos. Mag. **93,** 1132 (2013).

FIG. 1: (Color online) (a) Powder XRD pattern for $Gd_2Ir_2O_7$ at 300 K refined by the Rietveld method (the inset shows the all-in/all-out configuration of Ir^{4+} ions).
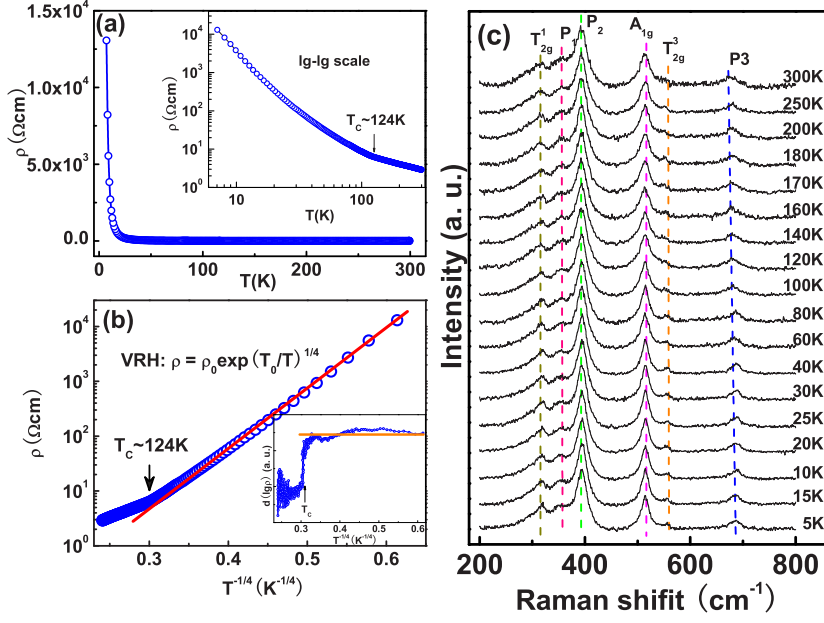
FIG. 2: (Color online) (a) The temperature dependence of resistivity $[\rho(T)]$ for $Gd_2Ir_2O_7$ (the inset plots on the $\lg-\lg$ scale); (b) the $\rho(T)$ curve fitted according to $T^{-1/4}$ law (the inset shows the derivative $\lg\rho(T)$ vs $T^{-1/4}$); (c) the Raman spectra at selected temperatures from 200 to 800 cm^{-1}
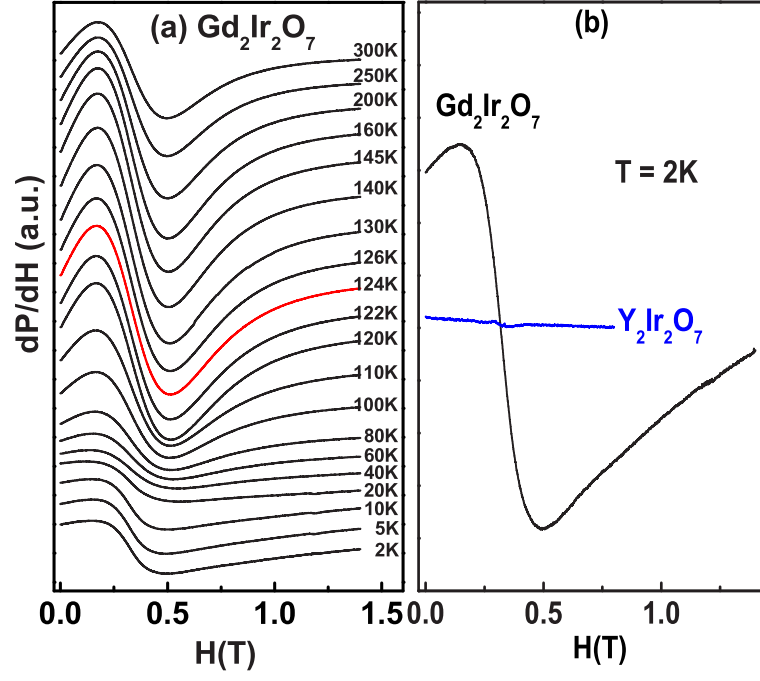
.

11

FIG. 3: (Color online) (a) The derivative EPR spectra (dP/dH) (P is the integral EPR intensity) for $Gd_2Ir_2O_7$ at selected temperatures; (b) the comparison of EPR spectra for $Y_2Ir_2O_7$ and $Gd_2Ir_2O_7$ at $T = 2$ K.
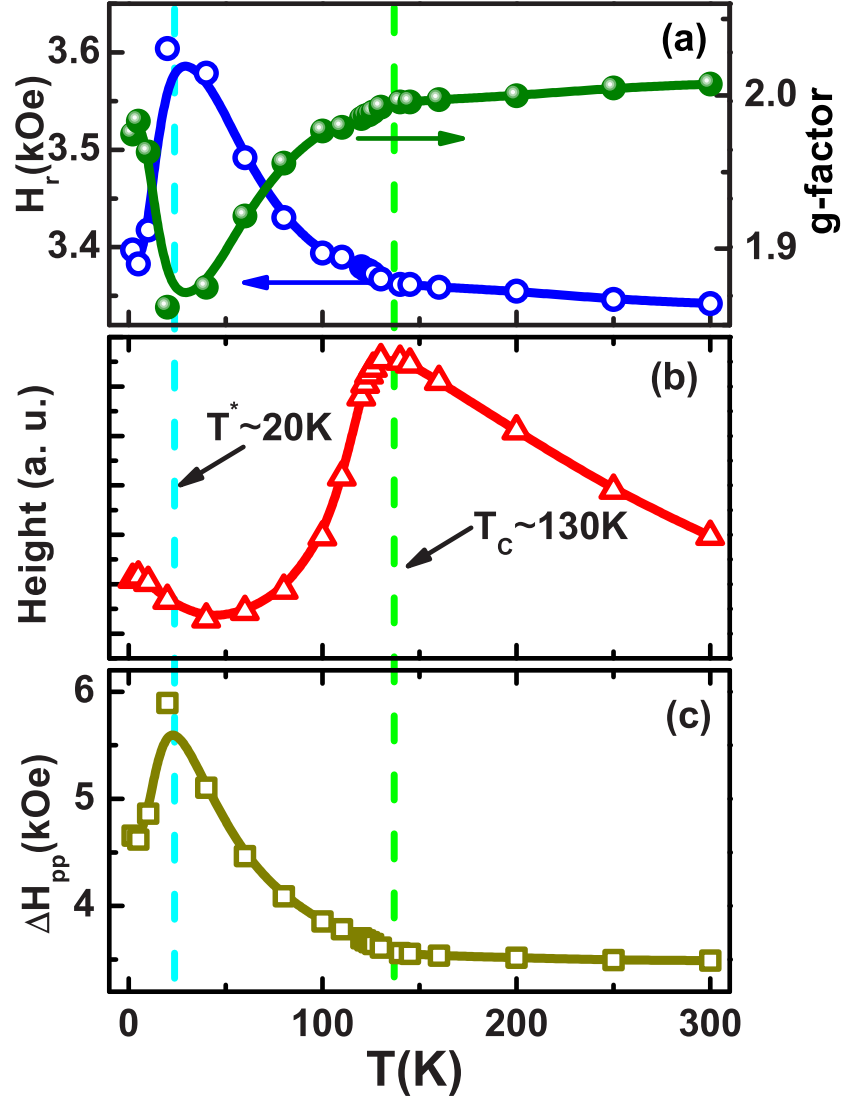
FIG. 4: (Color online) The temperature dependence of EPR parameters: (a) H_r and g-factor; (b) EPR height; and (c) ΔH_{pp}.
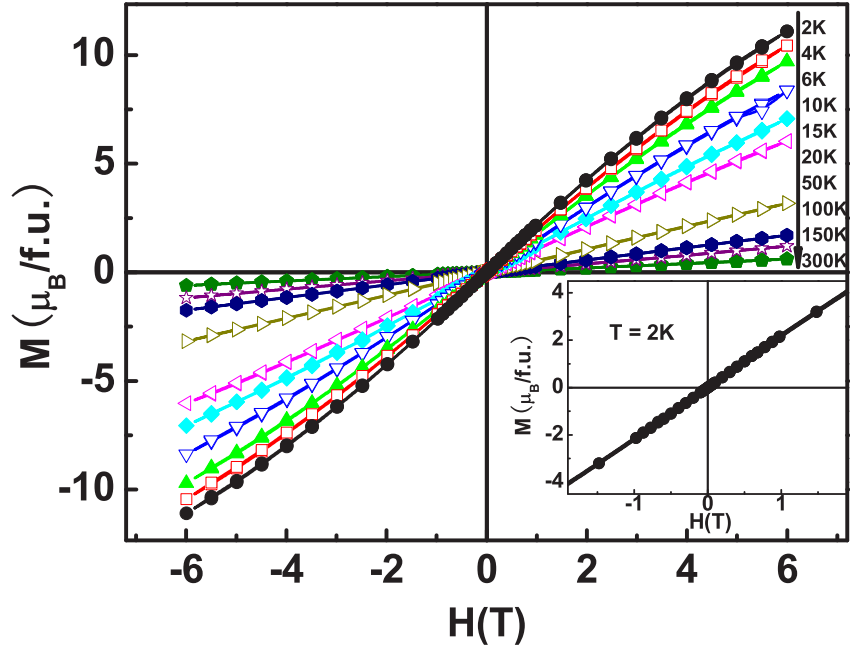
13

FIG. 5: The isothermal magnetization $M(H)$ at selected temperatures (the inset shows the magnification in the low field region at 2 K).
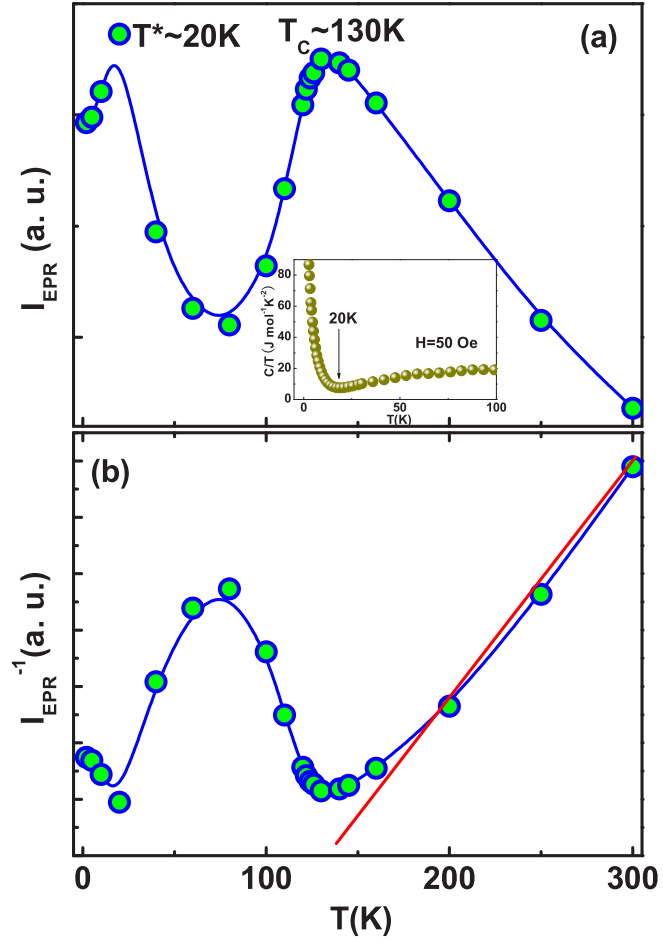
FIG. 6: (Color online) (a) The temperature dependence of I_{ESR} (the inset shows the specific heat $[C/T]$ vs T under $H =$ 50 Oe); (b) $I_{ESR}^{-1}(T)$ as a function of T (the line is guided on eye).